condensed matter

MDPI

Article

Hidden Universal Metal in Cuprate Superconductors

Abigail Lee and Jürgen Haase *

Felix Bloch Institute for Solid State Physics, University of Leipzig, Linnéstr. 5, 04103 Leipzig, Germany; abigail.lee@physik.uni-leipzig.de

* Correspondence: juergen.haase@uni-leipzig.de

Abstract

Nuclear relaxation, $1/T_1$, is a very robust probe of electronic excitations in superconducting materials above and below the critical temperature of superconductivity, T_c. Here, a relaxation phenomenology of hole-doped cuprate superconductors is presented based on the majority of the available literature data from the CuO_2 plane, without assumptions with respect to a hyperfine scenario, form factors, or particular theoretical models. Below a temperature similar to the pseudogap temperature, Heitler–Teller-type relaxation is uncovered universally; i.e., the nuclear spin relaxation above T_c is only determined by the absolute temperature, $1/T_1 \propto T$. All materials condense out of this metal at T_c, below which relaxation drops even faster, as expected from conventional superconductors, albeit without a Hebel–Slichter peak. It is a 'hidden metal' in the sense that it has a vanishing uniform response and thus hardly affects the NMR shifts; it is also not seen in planar O relaxation. The hidden metal causes a temperature-independent but material-dependent planar Cu relaxation anisotropy that is strongly correlated with the size of T_c. Moreover, the rate measured with the field in the CuO_2 plane is nearly the same for all cuprates: $1/^{63}T_{1\perp}T \approx 25/\mathrm{Ks}$, where $1/^{63}T_{1\parallel}$ is mainly responsible for the change in anisotropy. Above the hidden metal, the relaxation behavior changes and can be described by an ordinary but renormalized metal, with a reduced Cu relaxation anisotropy. The relaxation phenomenology, which should hold clues to the so-called strange metal, is also discussed in the context of the two spin components previously uncovered in the shifts, as well as the pseudogap and relation to other probes. This new phenomenology should give a better foundation for the understanding of the cuprates.

Keywords: superconductivity; cuprates; NMR

1. Introduction

Nuclear spin-lattice relaxation ($1/T_1$), the rate of transfer of nuclear magnetic energy to the surrounding 'lattice' or thermal bath, is a fundamental probe of material properties [1]. For metals, the unique electronic statistics also leads to a robust nuclear relaxation law, $1/T_1 \propto T$. This proportionality between rate and temperature was pointed out by Heitler and Teller in 1936 [2], a decade before NMR (nuclear magnetic resonance) in bulk materials was discovered. W. Knight found, in 1949, an NMR shift that was apparently special to metals [3], the temperature-independent Knight shift (K). This led Korringa in 1950 [4] to investigate how the Knight shift and Heitler–Teller relaxation are related in a Bloch-type metal. He found that in the absence of correlations, $1/T_1T = (\gamma_n/\gamma_e)^2 4\pi k_B/\hbar \cdot K^2$, which is the celebrated Korringa relation for simple metals. He also noted that electronic correlations are expected to affect shift and relaxation in fundamentally different ways. Therefore, the actual relation between

Check for updates

Academic Editor: Sergio Caprara

Received: 3 July 2026
Revised: 14 August 2026
Accepted: 19 August 2026
Published: 20 August 2026

Copyright: © 2026 by the authors. Licensee MDPI, Basel, Switzerland. This article is an open access article distributed under the terms and conditions of the Creative Commons Attribution (CC BY) license.

an NMR shift and relaxation aids in understanding the electronic state. In superconducting metals, below the superconducting transition temperature, T_c, shift and relaxation follow from BCS, and for spin-singlet pairing, both disappear rapidly below T_c, but a relaxation upturn just below T_c is predicted by BCS (the Hebel–Slichter coherence peak [5]). For a gap with nodes it can be much weaker or undetectable [6]. In any case, condensation does not affect the Heitler–Teller law described above T_c.

With the discovery of the superconducting cuprates [7], NMR shift and relaxation data were of great interest, in particular from ^{63,65}Cu and ^{17}O in the ubiquitous CuO_2 plane. Note that the nuclear spins couple to the electronic spins near the Fermi surface via magnetic hyperfine couplings. These depend on the nuclear site (Cu, O) in the rather large unit cell, and may not be well known. In the presence of more than one electronic spin, the hyperfine coupling scenarios can be even more complicated. In the absence of reliable theory, one can only seek reliable phenomenology.

Most early experimental information on shift and relaxation came from measurements of the $YBa_2Cu_3O_{6+y}$ class of materials [8–12]. They revealed a temperature-dependent shift for Cu, but only when the magnetic field (B_0) is in the plane, not when the magnetic field is pointed in the crystal c-direction ($c \parallel B_0$); e.g., in $YBa_2Cu_4O_8$. With an isotropic spin response, this can only happen if the shift from spin in the Cu $3d(x^2 - y^2)$ orbital (with the well-known coupling coefficient $A_\parallel$ being large and negative in related ionic salts) is accidentally offset by a second term. In a single-band picture, it was then assumed that $A_\parallel + 4B \approx 0$ and $A_\perp + 4B > 0$, with transferred Cu spin density of some isotropic coupling constant B, with the size determined by the cancellation requirement [12]. Of course, this hyperfine scenario also has profound consequences for understanding Cu nuclear relaxation. For example, it requires antiferromagnetic spin fluctuations along $c \parallel B_0$, as longer wavelengths are increasingly suppressed for $A_\parallel + 4B \approx 0$, preventing an unbiased view of the cuprates. The essential qualitative conclusions were spin-singlet pairing due to disappearing shift and relaxation below T_c and the presence of a spin gap or pseudogap, since some shifts are already temperature-dependent above T_c.

As data from more cuprates appeared in the literature, it became increasingly obvious that for most materials the Cu shift for $c \parallel B_0$ is also strongly temperature-dependent, overturning the old hyperfine scenario. Special tests of whether a single-spin-component view holds beyond $YBa_2Cu_4O_8$, $YBa_2Cu_3O_{6+y}$ [13,14] showed that that is not the case, since the shifts observed at different nuclei are not proportional to each other [15,16].

Very recently, using nearly all the literature shift data, it was shown that there are indeed two electronic spin components, A and B, at work. One, A, stemming from the Cu $3d(x^2 - y^2)$ spin, which sets the planar O as well as Cu axial shift, and another, B, Cu 4*s*-like spin that affects only planar Cu [17]. This conclusion was confirmed in a new, unbiased analysis of the NMR shifts which focused on the symmetry of the hyperfine coefficients only, not their size, and the doping and temperature dependence of the two shifts' components were summarized [18].

Here, we develop a phenomenology of nuclear relaxation in the hole-doped superconducting cuprates using nearly all the available literature relaxation data [19,20] (only $La_{2-x}Sr_xCuO_4$ is excluded due to its outlier behavior in terms of planar Cu, which will be discussed separately). We uncover the universal presence of Heitler–Teller-type metallic relaxation for planar Cu below a temperature similar to that of the pseudogap, T^*, cf. Figure 1. This means it is only the absolute temperature T that determines the nuclear relaxation rate $1/T_1$ in this region, apart from a temperature-independent but material-dependent relaxation anisotropy. As for conventional superconducting metals, at their respective T_c the cuprates condense out of this state. We call this region a 'hidden metal' since it lacks a sizeable uniform response, i.e., vanishing NMR shifts of Cu and O, and since it is not

easily detected at planar O, i.e., the 'hidden metal' does not follow the simple Korringa law. This 'hidden metal' has other intriguing properties. When measured through the hyperfine coefficients of Cu with the field perpendicular to the crystal c-axis, a rather similar rate is found for all cuprates, $1/^{63}T_{1\perp}T \approx 25/\mathrm{Ks}$. This is an astonishingly robust finding given that neither other chemical and electronic parameters nor crystal quality seem to interfere. Measured in the other direction, $1/^{63}T_{1\parallel}$ is proportional to $1/^{63}T_{1\perp}$ in the hidden metal, but it is material- and doping-dependent. Astonishing again is the fact that the T_c of a cuprate is correlated with this relaxation anisotropy, with the highest T_c at an anisotropy of about 1.9. It is therefore not surprising that this anisotropy correlates with the planar O hole content, previously measured with NMR [21–23], a correlation supported by very recent DMFT in the Emery model [24,25].

Above about T^*, the 'hidden metal' disappears and a renormalized metal emerges. This is the likely source for the metal-like, i.e., temperature-independent, shifts in the cuprates as well. This, and more details on the cuprate shifts [18], is an argument in favor of interpreting the cuprate relaxation in terms of a two-spin-component scenario.

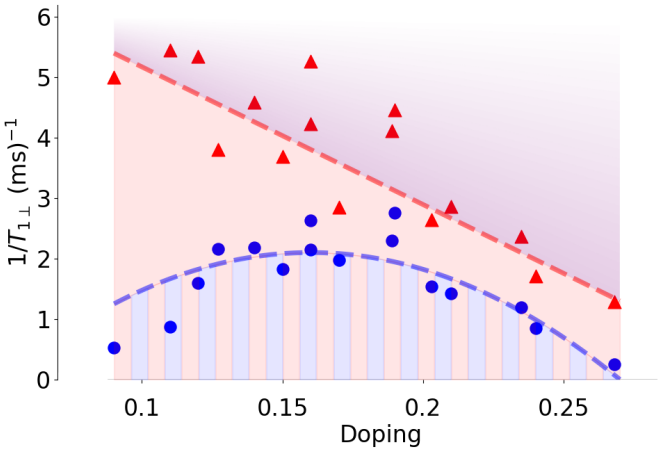


Figure 1. Nuclear relaxation rate $1/T_{1\perp}$ of planar Cu as a function of doping for many different cuprates (16 from 7 families). Note that in the hidden-metal (red shaded) region, $1/T_{1\perp}T$ is very similar for all, and we use a mean value of 25/Ks (see main text for details). Blue circles mark the relaxation rate with which a material enters this hidden-metal region above T_c; red triangles mark the rate above which it departs from it, i.e., where it begins to lag behind the universal metal relaxation. Both of these boundaries are defined by the temperature points at which the relaxation deviates by 6% from the metallic rate, but are relatively insensitive to the precise cutoff choice (see Appendix A). The red-shaded area thus approximates the temperature-doping region of this special metal. Within this region, the relaxation anisotropy is temperature-independent. Note that the condensate (red–blue-striped region) always forms out of this metal. Above the red triangles (approximated by the purple-shaded region), we see a renormalized two-component metal. The dashed red line is a linear guide to the eye; the blue dashed parabola is an adaptation of the T_c-doping relation [26]. Within the hidden metal, the relaxation rate can be directly translated into temperature, resulting in the similarity in appearance to the temperature-doping phase diagram. Note that the points are not normalized with respect to the family-dependent $T_{c,max}$, resulting in some scatter.

2. Nuclear Relaxation

Planar ^{63}Cu spin relaxation is either reported with the external magnetic field along the crystal c-axis ($c \parallel B_0$) or perpendicular to it ($c \perp B_0$). The former measures $1/^{63}T_{1\parallel}$ (relaxation of ^{63}Cu due to in-plane fluctuating fields, perpendicular to the c-axis, which are also measured in NQR); the latter measures $1/^{63}T_{1\perp}$ (due to both out-of-plane and in-plane fluctuating fields), independent of in-plane axis rotation due to symmetry. The anisotropy of ^{63}Cu spin relaxation, $^{63}R = {}^{63}T_{1\parallel}/{}^{63}T_{1\perp}$, is expected to yield information about the

anisotropy of the hyperfine coefficients, as the electronic spin is isotropic. A summary of typical experimental data is shown in Figure 2a,b, cf. [19], and we return to the analysis after introducing the planar O data.

A crude phenomenology of planar ^{17}O nuclear spin relaxation in all cuprates was presented recently [20]. It could be modeled with a universal metal and a temperature-independent, but doping-dependent, pseudogap. When measured with the field along the crystal c-axis, one finds $1/^{17}T_{1c}T \approx 0.40/\mathrm{Ks}$ beyond the doping $x \simeq 0.2$ for all materials, cf. Figure 2d (for more data, see [20]). The same metallic behavior is found even at lower doping levels, albeit at increasingly higher temperatures and with an offset. Furthermore, the simple Korringa relation appears to hold, with a metallic shift of about 0.25% [20]. The anisotropy is largely material-independent and expected by the hyperfine coefficients; therefore, one can focus on the most abundant data for $c \parallel B_0$. Planar O thus points to a rather well-defined simple, universal metal in the cuprates, except that below about $x \simeq 0.2$ it lacks low-energy states due to a temperature-independent pseudogap, obscuring the condensation behavior [20].

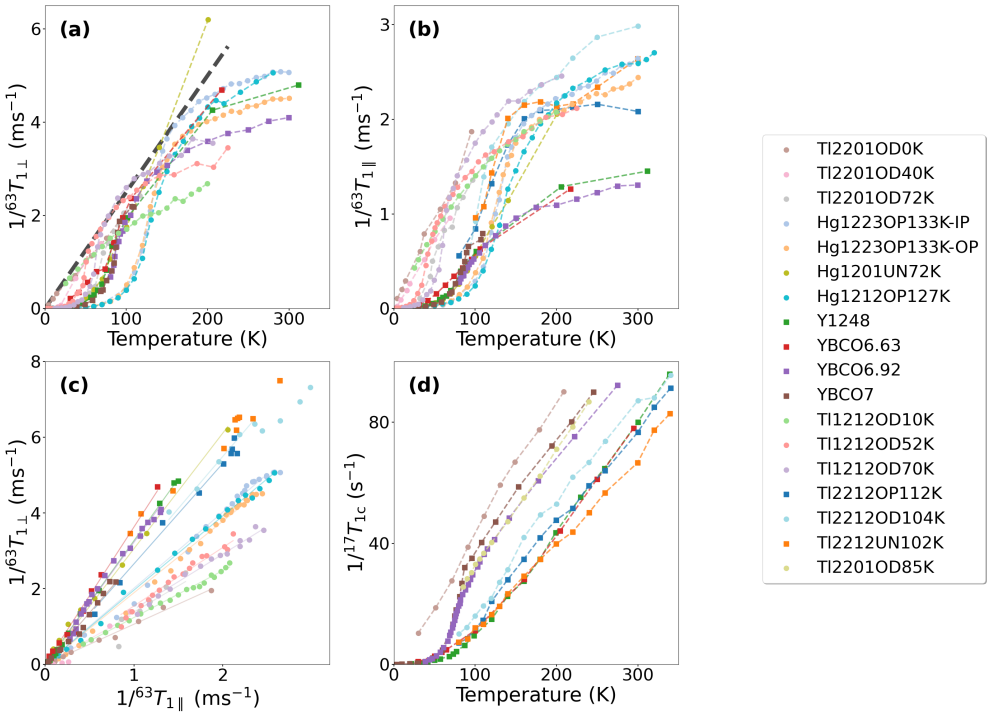


Figure 2. Nuclear relaxation in 18 different hole-doped cuprates. (**a**) $1/^{63}T_{1\perp}$ vs. T (field applied perpendicular to the crystal c-axis). The gray dashed line marks a rate of 25/Ks. (**b**) $1/^{63}T_{1\parallel}$ vs. T (field applied along the crystal c-axis) shows a much larger variation between family and doping. (**c**) A plot of $1/^{63}T_{1\perp}$ vs. $1/^{63}T_{1\parallel}$ with temperature as an implicit parameter. This relaxation anisotropy is material- and doping-dependent, but temperature-independent within a certain window above T_c [19]. The variation in relaxation anisotropy is primarily set by the changes in $1/^{63}T_{1\parallel}$. (**d**) Planar oxygen relaxation $1/^{17}T_{1c}$ (subscript c for $c \parallel B_0$) follows what appears to be a simple metallic behavior, albeit with a gap in the low-energy DOS at lower doping levels [20]. Much of the data displayed for Cu and O alike have been presented cumulatively before [19,20]. Note that the Tl-2212 family is omitted from panel (**a**) as $1/^{63}T_{1\perp}$ was not measured directly but rather deduced from spin-echo decay. Original sources for the data can be found in Table A1 in Appendix A.

Returning to Cu relaxation, Figure 2a,b reveal a very different picture. The salient features are the following. First, we notice that T_c is easily visible in the bare data for all materials in Figure 2a; it is also present for $c \parallel B_0$, although not as easily seen in Figure 2b. Apparently, the pseudogap behavior does not obscure the onset of condensation, as for O, and one can measure $1/T_1$ near T_c (blue points in Figure 1).

Second, $1/^{63}T_{1\perp}$ near T_c is found on very similar metallic ($1/T_1 \propto T$) lines, i.e., $1/^{63}T_{1\perp}T_c$ is rather similar for all cuprates (relative standard deviation of 9% for the measured rates; see Appendix A for details). However, the relaxation measured along the crystal c-axis, $1/^{63}T_{1\parallel}$, varies significantly between materials, including near T_c. It has been noted before [19] that this relaxation anisotropy, cf. Figure 2c, is temperature-independent (within the red-shaded region of Figure 1), but does depend on doping and family. It has the tendency to become more isotropic at high doping levels, and can be as large as 3.6 for certain materials at lower doping levels.

Third, the range of temperatures over which the relaxation rate of a particular material stays on its metallic line is doping-dependent. In order to investigate this in more detail, it is useful to normalize all metallic lines for $c \perp B_0$, since slight differences in the slope obscure, in terms of the actual rate, how large the temperature range is over which a material follows the metallic slope. For that reason, we set the slopes to $1/^{63}T^*_{1\perp}T = 25/\mathrm{Ks}$. This value corresponds to the mean value of $1/^{63}T_{1\perp}T$ in this region for all materials presented here (a mean of 22.7/Ks is obtained considering only materials for which $1/^{63}T_{1\perp}$ was directly measured; see Appendix A for details). The precise value is less important here than the observation that the cuprates have a very similar $1/^{63}T_{1\perp}T$, despite the data coming from groups around the world, on all sorts of cuprates, with different 'sample quality'. This rate is indicated by the dashed line in Figure 2a. This behavior is easily observed in Figure 3, where we further normalize all $1/^{63}T^*_{1\perp}$ by the reported T_c, i.e., the temperature-dependent rates, $1/^{63}T_{1\perp}T$, are shifted to fixed T_c and multiplied by T_c. Apart from the drop near T_c, there is universal metallic behavior up to $T_▲$, cf. Figure 1. Above $T_▲$, the relaxation lags behind the Cu hidden-metal rate.

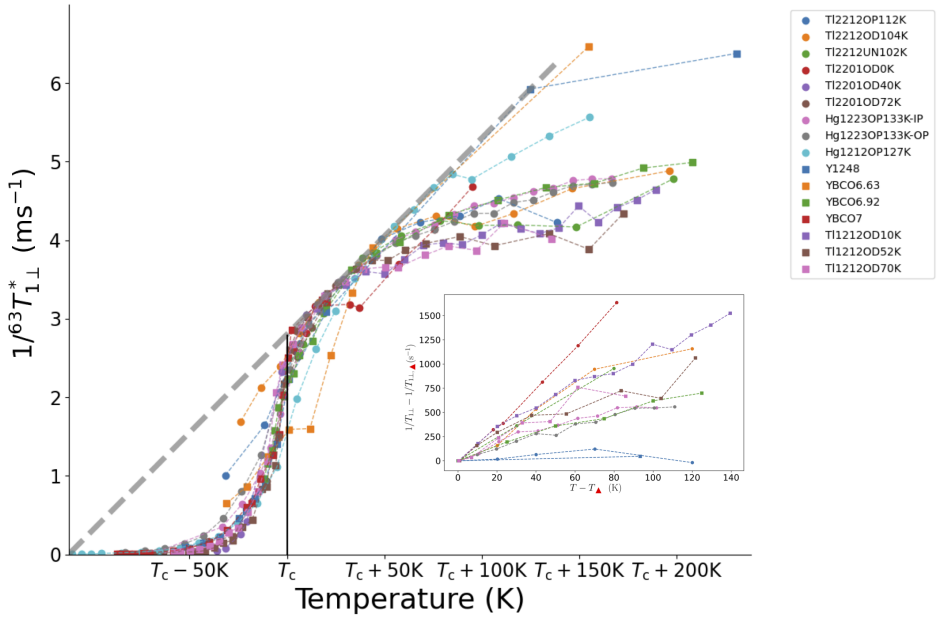


Figure 3. Main panel: Scaled temperature dependence of Cu relaxation from Figure 2a. The scaled $1/^{63}T^*_{1\perp}$ is plotted as a function of a shifted temperature axis such that the quoted T_c for each material is aligned to the black vertical line. $1/^{63}T^*_{1\perp}T$ ($1/^{63}T_{1\perp}T$ adjusted to fit $1/^{63}T_{1\perp}T = 25/\mathrm{Ks}$; dashed gray line in the figure) is multiplied by the shifted $T = T_c$ (see main text for details). This serves as a visual aid to highlight the universality of the relaxation below $T_▲$. Above T_c, materials follow this metallic (dashed gray) line for a doping-dependent finite window in temperature before turning off. Note that given the proportionality, a similar curve can be obtained from $1/^{63}T_{1\parallel}$ if additionally scaled by the observed relaxation anisotropies. Inset (lower-right panel): Unscaled $1/^{63}T_{1\perp} - 1/^{63}T_{1\perp▲}$ vs. $T - T_▲$, where the red triangle denotes rate and temperature at the red triangles in Figure 1, i.e., at the onset of the hidden metal. In this region, the relaxation anisotropy deviates from the temperature-independent values seen in the lower-temperature region. Dotted lines are guides to the eye. Hg1201UN72K is omitted here due to uncertainty in the scaling factor.

In the hidden-metal region, the relaxation anisotropy, ^{63}R, varies with doping and family, but is independent of temperature [19]. Thus, while $1/^{63}T_{1\parallel}$ behaves differently from $1/^{63}T_{1\perp}$, we would find the same universal temperature dependence in this region of the phase diagram if we multiplied $1/^{63}T_{1\parallel}$ by ^{63}R. At higher temperatures, above the hidden-metal line, the relaxation anisotropy decreases for all materials shown here. This high-temperature addition to the relaxation for $c \perp B_0$ is isolated in the inset of Figure 3 (lower-right panel). Note that the fixed anisotropy within the hidden-metal line is not expected to strictly apply to the superconducting state, for which the relaxation behavior will be governed by a different functional dependence compared to that of the hidden metal.

Most remarkably, the relaxation anisotropy measured on the hidden metal can be directly related to T_c, as shown in Figure 4. The highest-T_c materials have a relaxation anisotropy of $^{63}R \approx 1.9$. The family dependence of T_c is reflected in the relaxation anisotropy; optimally doped materials with a lower T_c lie at either higher or lower anisotropy, depending on the family, but fall on the same lines as the non-optimally doped samples. There is apparently an ideal makeup of the hidden metal, from which the superconducting state emerges, which correlates with a high T_c.

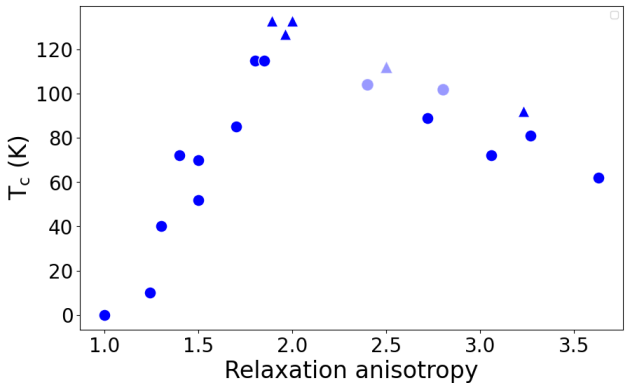


Figure 4. Quoted value of T_c plotted against the Cu relaxation anisotropy (^{63}R) within the hidden-metal region for 20 different materials and doping levels. Optimally doped materials within a given family are marked with triangles instead of circles, and the faded data points indicate members of the Tl-2212 family, for which $^{63}1/T_{1\perp}$ was not directly measured (see Appendix A for details). Increased doping within a family decreases the relaxation anisotropy. Note that members of the $YBa_2Cu_3O_{6+y}$ family show significantly larger relaxation anisotropies compared to other materials at similar doping levels, including the optimally doped compound, but nevertheless lie on the same curve. For a list of material-dependent anisotropies, see Table A1 in the Appendix A. The anisotropies plotted here result from the true, unscaled relaxation data, and the fitting error in the anisotropy is $\leq$0.035 where it is not quoted directly from the literature (note that there is more data available for the relaxation anisotopy compared to the full hidden-metal temperature range). Spearman rank-correlation statistics for the relation between T_c and ^{63}R can be found in Table A2 in the Appendix B, along with a family-sorted version of this figure.

3. Discussion

We begin the discussion by characterizing the three regions in the cuprate phase diagram, cf. Figure 5, with observations from planar Cu and O relaxation. Thereafter, we discuss the possible consequences for the NMR shifts that were recently discussed by us in terms of two-spin components [18]. Finally, we enter a broader discussion involving other probes.

It is very important to stress that the discussion of the distinct regions (I, II, III) in the cuprate phase diagram does not invoke particular hyperfine scenarios, form factors, or other particular theoretical models. Region I in Figure 5 is characterized by the 'hidden metal', Region II begins with condensation from the hidden metal into the superconducting

state at T_c. Region III, defined by the temperature T^*, in Figure 5, where the Cu relaxation rate departs from that of the hidden metal, appears as a renormalized metal.

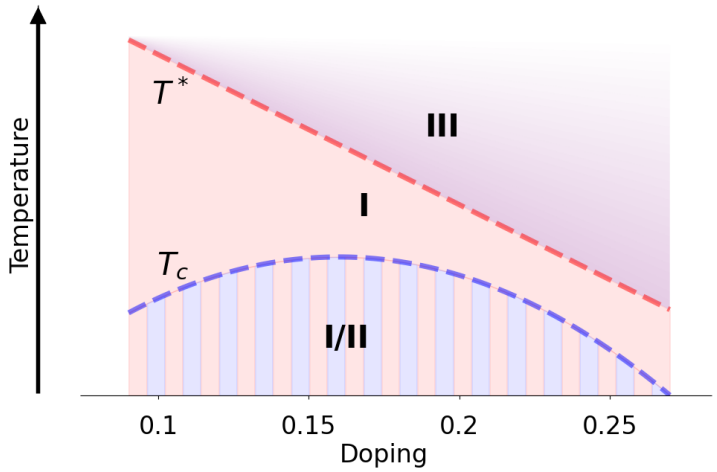


Figure 5. Schematic diagram of the different regions defined by planar Cu nuclear relaxation overlaid on the cuprate phase diagram. The hidden metal dominates region I (red). The striped region below the blue dashed line indicates the superconducting state (II) that forms out of this special metal. Region III is governed by a different, apparently renormalized two-component metal with temperature $T - T^*$, where T^* is defined as the temperature at which the Cu relaxation behavior changes (see text for details). The hidden metal should persist down to $T = 0$ were the superconducting state not to intervene; therefore, we label the dome as region I/II.

3.1. Superconducting Hidden Metal (I and I/II)

Below T^* in Figure 5, the electronic matter causes metallic planar Cu relaxation (in the Heitler–Teller sense), and below T_c, the relaxation suddenly drops out of this hidden metal. There is no Hebel–Slichter peak (this is expected for predominantly *d*-wave pairing in conventional metals [6,27]). This sharp drop in the Cu relaxation near T_c is consistent with the onset of the superconducting state. The concrete properties of the metallic state are the following. First, the relaxation rate for $c \perp B_0$, i.e., measured with the magnetic field in the plane, is very similar for all cuprates, $1/^{63}T_{1\perp}T \approx 25/\mathrm{Ks}$, indicating some sort of fundamental property of the cuprates. The rate measured along the crystal *c*-axis is, in contrast, strongly family- and doping-dependent, but remains proportional to the rate measured in the other direction, as one would assume. Astonishing is the relation of the relaxation anisotropy to T_c of the particular cuprate, cf. Figure 4. Unlike the doping dependence of T_c in the regular phase diagram, the anisotropy sorts T_c not according to family but across all cuprates. In other words, the electronic matter contains information about the temperature at which condensation occurs. Note that this relaxation is observed up to the highest doping levels. For the most overdoped sample, in the absence of T_c, the hidden metal remains from the red dashed line down to the lowest temperature.

The hidden metal does not significantly contribute to the relaxation of the planar O nucleus below a doping of about $x \approx 0.2$, as its rate, $1/^{17}T_1$, decreases due to missing electronic states from the opening of a temperature-independent pseudogap. As doping increases, the states lost to the pseudogap are apparently fully recovered already well before the end of the superconducting dome, and the relaxation rate turns simply metallic, with a universal value of about 0.40/Ks for all cuprates. It appears, in this crude picture, that the pseudogap for planar O closes at a significantly lower doping level compared to the end of the hidden metal, and the superconducting gap becomes visible. The metallic relaxation of about 0.40/Ks is small compared to the 25/Ks of the hidden metal.

3.2. Renormalized Metal (III)

The planar Cu relaxation behavior changes rather abruptly from that of the hidden metal upon crossing the red dashed line in Figure 5. The relaxation rate suddenly begins to lag behind that of the hidden metal, cf. Figure 2a,b and the main panel of Figure 3. Interestingly, if we plot the renormalized relaxation, i.e., vs. temperature $T - T^*$, we find simple metallic behavior, as seen in the inset to Figure 3.

For planar O, the relaxation is nearly universal, and its behavior can similarly be explained with a renormalized relaxation that apparently starts with the opening of the pseudogap. Thus, the renormalization of planar O relaxation seems to be related to the loss of states to the pseudogap. However, since planar O sees a much lower relaxation rate than Cu, ongoing renormalization may be difficult to observe. Meanwhile, the renormalized relaxation rate of Cu continues to increase with doping until at least the end of the superconducting dome. It appears that since the states below T^* are lost to another phase, the description of region III in terms of renormalization is a useful description.

3.3. Relation to the Cu and O NMR Shifts

Previously, we showed that the planar Cu shifts can be described as the sum of an anisotropic shift, $^{63}K_A$, and an isotropic shift, $^{63}K_B$, even without considering specific values for the associated hyperfine coefficients, based solely on their symmetry [18]. Such a decomposition of the shifts was motivated by the fact that planar Cu sees an isotropic shift contribution which does not affect planar O, and which carries a different temperature dependence [17]. This analysis further showed that these hyperfine coefficients must be quite similar across materials. This point is important, for it demonstrates that changes to shift and relaxation must stem from the underlying electronic matter, rather than variations in the hyperfine coefficients through which the electronic spins couple to the nuclei.

The newly defined regions of the phase diagram also offer new insight into the shift behavior. The doping-dependent high-temperature metallic plateaus of $^{63}K_A$, and also of $^{17}K_\alpha$, were found to saturate to a maximum value near $x \gtrsim 0.2$. This is the same doping above which planar O relaxation appears as purely metallic without renormalization. In contrast, the high-temperature plateau of $^{63}K_B$, which is only seen by planar Cu, increases with doping until at least the end of the superconducting dome, much like the renormalized relaxation rate. Thus, the high-temperature metallic shift plateaus may be a consequence of renormalization rather than a change in density of states (in the simple metallic sense). The contrast in the doping dependence of the renormalization, as seen by Cu and O relaxation, could thus be evidence of two-component behavior that is independent from the previously noted shift evidence.

If we examine the renormalized scaling, we find that the Cu relaxation rate approximately obeys the simple Korringa relation if one considers the two shift components individually, as in $^{63}K_A^2 + {}^{63}K_B^2$. For the most highly overdoped (non-superconducting) sample, this yields a metallic relaxation of 18/Ks, similar to the measured value of 20/Ks of the renormalized metal above T^*. Decreasing doping tends to decrease the high-T slopes, consistent with the decreasing high-temperature shift components. This suggests that the states above T^* present themselves as two uncorrelated metals.

Understanding the relationship between the shifts and relaxation in the hidden metal (region I) may be more complicated. The abrupt changes observed in the relative temperature dependences of the two shift components should be connected to the phenomenology presented here, but are difficult to explain without suitable theory. For most of this region, both shift components are also disproportionately small with respect to the Cu relaxation compared to what one would expect for an ordinary, uncorrelated metal. In the underdoped materials, there is no sharp drop in the planar Cu and O shifts at T_c, which are

already temperature-dependent and decreasing above the transition. For a hidden metal with little or no shift condensing into a spin-singlet superconductor (which also lacks shift), the lack of a clear drop at T_c is expected, as the temperature dependence of the shifts is primarily governed by the renormalized metal above and the Fermi function. T_c is not visible in the planar O relaxation of the underdoped materials either. Meanwhile, the drop in relaxation of planar Cu near T_c from the hidden metal rate remains quite sharp.

Deviations from the Korringa relation for an uncorrelated metal between shift and relaxation, such as those seen in the hidden-metal region, should provide information regarding correlations present in the system. To produce the behavior of the shifts in the hidden metal, such correlations should strongly reduce the uniform spin susceptibility of the system.

Finally, we would like to note that the observation of an apparently optimal relaxation anisotropy, similar to the previously observed matching condition between the Cu shift components [17]. The matching condition in the Cu shift components seems to relate to optimal doping, but not the family-dependent $T_{c,max}$ that is observed in the relaxation anisotropy.

3.4. General Remarks and Further Discussion

As shown in Figure 4, the relaxation anisotropy of the hidden metal seems to be an important parameter with respect to T_c. It carries information similar to that given by the sharing of the total hole content determined with NMR, which shows that the maximum T_c of the cuprates is proportional to the planar O charge at optimal doping [23,28]. This was also found with very recent cellular DMFT [24,25]. In Figure 6 we show the correlation between the Cu relaxation anisotropy and the planar O hole content for both optimally and non-optimally doped materials.

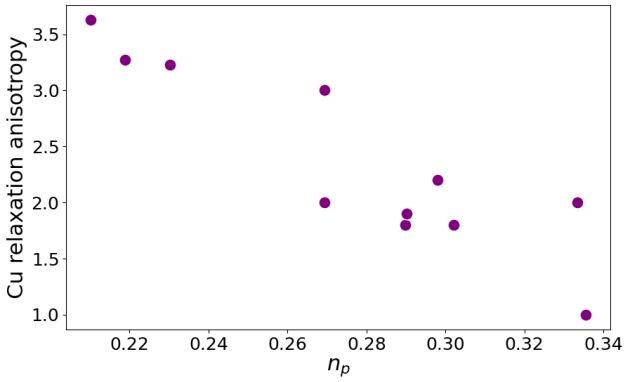


Figure 6. Planar Cu relaxation anisotropy (^{63}R) decreases with increasing planar O hole content n_p. Planar O quadrupole splittings are taken from [23], wherein it was also shown that the planar O hole content at optimal doping correlates with $T_{c,max}$. Note that this planar O hole content includes both the doped as well as shared parent hole [22].

We note that $La_{2-x}Sr_xCuO_4$ has been excluded from the phenomenology presented here, as analysis of this family is complicated by an additional shift component of axial symmetry on planar Cu [17], for which the contribution to relaxation is not known. However, we note that the planar O shift and relaxation in these materials are apparently unaffected by this additional contribution and are similar to the other families [20]. A deeper understanding and analysis of its planar Cu relaxation remains an important topic for future work, especially given that it is possible to measure up to very high temperatures, where the behavior may change [29].

The red dashed T^* line in Figure 5 is similar in its doping dependence to the pseudogap line defined by the planar O shift [20] or entropy [30], but how the two may be related is not entirely clear. It seems that the renormalization of the two spin components as

a function of doping is not identical. Planar O relaxation is only affected by one spin component. The renormalization of the O relaxation and the pseudogap end at the same doping. The hidden-metal relaxation of Cu, which is affected by both spin components, is seen both in materials with a pseudogap in the normal state as well as in strongly overdoped materials without a clear gap in the density of states. In fact, the hidden metal persists until the end of the superconducting dome at high doping, as does the renormalization. It is also worth noting that multicomponent models can lead to component- and probe-dependent behavior. For example, intercomponent coupling in a pairing-based multicomponent model can screen, enhance, or redistribute pseudogap signatures between components [31]. This mechanism is distinct from our phenomenological two-spin-component description, but may provide a useful conceptual context for the different temperature and doping dependence observed in the Cu and O shift and relaxation. Perhaps the hidden metal is involved in the formation of the pseudogap state, or maybe both phenomena originate from a common underlying electronic reconstruction. It could also be that the hidden metal tracks a different parameter, such as a doping-dependent saturation of spin correlations or magnetic crossover into a correlated metal [32–34], rather than the pseudogap crossover itself. This distinction may be important, particularly in considering planar O relaxation, which apparently experiences little of the hidden-metal contribution. The characterization of the relaxation across the phase diagram, particularly in region III, may also be useful for the understanding of the strange metal scenario. Finally, we note that the line sketched between regions I and III in Figure 5 would extrapolate at zero doping to a value near T_N, but there is not enough available data at low doping beyond $La_{2-x}Sr_xCuO_4$ to explore this further at the present time.

The phenomenology presented here should be related to observations from other probes. For example, STM [35] and specific heat [30,36] also show a temperature-independent pseudogap that closes as a function of doping. These are expected to weight the antinodal regions near the saddle point more heavily [37], as does planar O relaxation, given the form factor, which also suppresses fluctuations near the antiferromagnetic wavevector. Transport data, on the other hand, is known to weight the nodal regions more heavily, where ARPES observes coherent quasiparticles [38,39], and shows metallic ($\rho \propto T^2$) behavior in the pseudogap region [40]. Considering the theoretical form factors for planar Cu hyperfine coupling [12,41], this should be related to the hidden metal we describe here. One might also expect that near universality of the planar Cu 25/Ks hidden-metal relaxation, paired with the changing relaxation anisotropy, should be tied to the shifting distribution of spectral weight in q-space seen by neutron scattering [42,43] and optical conductivity [44]. It is not clear at present what role charge and spin inhomogeneities, which have been observed in the NMR data [45], play in this phenomenology. The role of the lattice [46] also remains as an avenue of further discussion, including what the isotope effect [47] on the hidden metal or the renormalization is. We would also like to note that the two-component phenomenology presented here may invite analogies to Kondo lattice physics.

In summary, we have uncovered, through planar Cu relaxation, three regions of the phase diagram of hole-doped cuprates. Region I is described as a hidden metal, wherein Cu obeys Heitler–Teller-type relaxation rather universally. The Cu relaxation anisotropy in this region correlates with T_c and thus the planar O hole content. It is interesting to note that the rate for $c \perp B_0$, $1/{}^{63}T_{1\perp}T \approx 25/\mathrm{Ks}$, is very similar for all materials, while that for $c \parallel B_0$, $1/{}^{63}T_{1\parallel}T$, is largely responsible for the change in anisotropy. The hidden metal predominantly shows a small or vanishing uniform response as measured via the spin shifts, in contrast to the behavior of an ordinary metal. Superconductivity (region II) always emerges from this hidden metal, regardless of whether the material is under-

or overdoped, independent of structural differences, sample quality, or other material-dependent properties. Finally, region III is described by a renormalized metal above T^*. It appears to consist of two metallic spin components. Planar O relaxation is only affected by one spin component, and is only renormalized up to a doping of $x \approx 0.2$, concurrent with the end of the pseudogap. In contrast, the renormalization of planar Cu, which is affected by both spin components, continues until at least the end of the superconducting dome ($x \gtrsim 0.27$). This phenomenology demonstrates the importance of considering the hole-doped cuprates cumulatively, and should provide profound clues to aid in the development of the microscopic theory of the cuprates.

Author Contributions: A.L. performed all data analysis. A.L. and J.H. contributed equally to preparing the manuscript. J.H. had the overall leadership. All authors have read and agreed to the published version of the manuscript.

Funding: Funding of the research came from Leipzig University.

Data Availability Statement: All used data will be made available which enables reproduction of the results.

Acknowledgments: We acknowledge financial support from Leipzig University, in particular Roger Gläser, and stimulating scientific discussions with Nabeel Aslam. We also thank Steve Conradson and Takeshi Egami for valuable feedback.

Conflicts of Interest: The authors declare no conflicts of interest.

Appendix A. Literature Data

Table A1 contains the references for all the literature data used in this analysis. The values listed in the doping column for single- and bi-layer materials are those one finds if estimating from the parabolic dependence of T_c on doping alone [26], while those listed for multilayer materials are taken as given from the reference where available. UD, OP, and OD in the material labels stand for underdoped, optimally doped, and overdoped, respectively, and are followed by the quoted value of T_c. Materials with distinct inner and outer CuO_2 planes are labeled additionally with -IP and -OP to signify data pertaining to the inner and outer planes, respectively. $T_▲$, at which the relaxation rate is shown in Figure 1, is determined from the highest temperature for which the scaled $1/^{63}T_{1\perp} \geq 23.5$/Ks (6% deviation). Further columns give the values for 4% and 8% deviation cutoff values to demonstrate that the results are not significantly dependent on the chosen cutoff. These values are the lower bounds for Hg1201UD72K and YBCO6.63, since the high-temperature bend in $1/^{63}T_{1\perp}$ is not clear within the temperature range for which data were available. Planar O quadrupolar splitting can be found in Ref. [23].

Among the directly measured relaxation rates for $c\perp B_0$ within the hidden-metal region, the standard deviation is ± 2/Ks and the relative standard deviation is 9%. The mean relaxation rate for $c\perp B_0$ of all materials is 25/Ks; excluding the inferred rates of Tl-2212, it is 22.7/Ks. Since the precise value used for normalization of the relaxation rates merely changes the scaling factor and does not affect the phenomenolgy, we use 25/Ks for the normalization and discussion throughout for simplicity.

Table A1. List of materials, extracted data, and data references used in the analysis.

Material	Formula	Doping x	Ref. $1/^{63}T_1$	Scaling factor $1/^{63}T_{1\perp}T$	$1/^{63}T_{1\perp}T$ $(\mathrm{Ks})^{-1}$	^{63}R ($\pm$0.035)	$^{63}T_{\blacktriangle}$ (6%) (K)	$^{63}T_{\blacktriangle}$ (4%) (K)	$^{63}T_{\blacktriangle}$ (8%) (K)	Ref. $1/^{17}T_1$
Hg1201UD72K	$HgBa_2CuO_{4+\delta}$	0.09	[48]	-		3.1	$\geq$200	$\geq$200	$\geq$200	[49]
Tl2201OP85K	$Tl_2Ba_2CuO_{6+y}$	0.16	[50]	-	-	1.6 [a]	-	-	-	[50]
Tl2201OD72K	$Tl_2Ba_2CuO_{6+y}$	0.2	[51]	1.18	21.2	1.4	116(20)	116(20)	116(20)	-
Tl2201OD40K	$Tl_2Ba_2CuO_{6+y}$	0.24	[51]	1.23	20.3	1.3	69(12)	69(12)	69(12)	-
Tl2201OD0K	$Tl_2Ba_2CuO_{6+y}$	0.27	[51]	1.1	22.8	1	14(10) [c]	14(10) [c]	14(10) [c]	[52]
Tl1212OD70K	$TlSr_2CaCu_2O_{7-\delta}$	0.21	[53]	0.94	26.6	1.5	117(10)	117(10)	117(10)	-
Tl1212OD52K	$TlSr_2CaCu_2O_{7-\delta}$	0.23	[53]	0.99	25.2	1.5	104(10)	95(10)	104(10)	-
Tl1212OD10K	$TlSr_2CaCu_2O_{7-\delta}$	0.265	[53]	1.15	21.7	1.25	50(10)	40(10)	50(10)	-
YBCOUN62	$YBa_2Cu_3O_{6.63}$	0.11	[13]	1.12	22.3	3.6	$\geq$217	$\geq$217	$\geq$217	[13]
YBCO6.92	$YBa_2Cu_3O_{6.92}$	0.14	[54]	1.14	21.9	3.2	138(12)	138(12)	150(12)	-
YBCO6.96	$YBa_2Cu_3O_{6.96}$	0.16	-	-	-	-	-	-	-	[55]
YBCO7	$YBa_2Cu_3O_7$	0.17	[56]	1.21	20.7	2.7	-	-	-	[57]
Y1248	$YBa_2Cu_4O_8$	0.12	[58]	1.21	20.7	3.3	205(40)	205(40)	205(40)	[14]
Tl2212UN102K	$Tl_2Ba_2CaCu_2O_{8-\delta}$	0.127	[59] [b]	0.64	39	2.8	160(20)	140(20)	160(20)	[59]
Tl2212OP112K	$Tl_2Ba_2CaCu_2O_{8-\delta}$	0.16	[59] [b]	0.86	32	2.5	180(20)	160(20)	180(20)	[59]
Tl2212OD104K	$Tl_2Ba_2CaCu_2O_{8-\delta}$	0.189	[59] [b]	0.71	29.7	2.4	160(20)	160(20)	160(20)	[59]
Hg1212OP127K	$HgBa_2CaCu_2O_{6+\delta}$	0.16	[60]	1.15	21.7	1.95	210(10)	210(10)	220(10)	-
Tl2223OD115K-IP	$Tl_2Ba_2Ca_2Cu_3O_{10-\delta}$	0.124	[61]	-	-	1.85	-	-	-	[61]
Tl2223OD115K-OP	$Tl_2Ba_2Ca_2Cu_3O_{10-\delta}$	0.196	[61]	-	-	1.8	-	-	-	[61]
Hg1223OP133K-IP	$HgBa_2Ca_2Cu_3O_{8-\delta}$	0.14	[62]	1.01	24.8	2	190(10)	180(10)	200(10)	[62]
Hg1223OP133K-OP	$HgBa_2Ca_2Cu_3O_{8-\delta}$	0.19	[62]	1.13	22.1	1.9	190(10)	180(10)	190(10)	[62]

[a] Relaxation anisotropy ^{63}R quoted from [50]. [b] $1/^{63}T_{1\perp}$ not measured directly but deduced from spin-echo decay. [c] $1/^{63}T_{1\perp}$ omitted from Figure 1 due to large error ratio.

Appendix B. Anisotropy Statistics

Table A2 contains Spearman rank-correlation statistics for the T_c versus Cu relaxation anisotropy data above and below different breakpoints in the anisotropy. Figure A1 is a family-sorted version of Figure 4 from the main text.

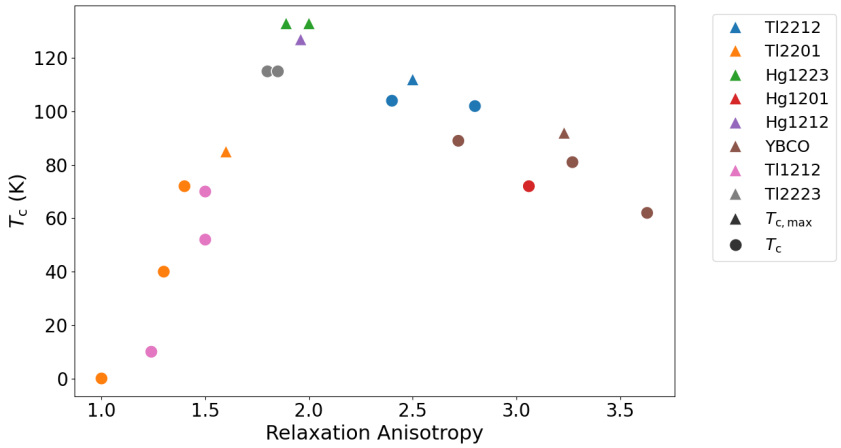


Figure A1. T_c vs. planar Cu relaxation anisotropy (^{63}R) from Figure 4 sorted by family.

Table A2. Spearman rank-correlation statistics for the T_c versus Cu relaxation anisotropy data for different anisotropy breakpoints.

Anisotropy Breakpoint	Branch	Spearman's ρ	p-Value	Number of Data Points
2.2	Lower	0.96	$<10^{-4}$	12
2.2	Upper	−0.81	1.5×10^{-2}	8
2	Lower	0.96	$<10^{-4}$	11
2	Upper	−0.87	2.5×10^{-3}	9
1.8	Lower	0.88	8×10^{-3}	7
1.8	Upper	−0.86	1.5×10^{-4}	13

References

1. Slichter, C.P. *Principles of Magnetic Resonance*, 3rd ed.; Springer: Berlin/Heidelberg, Germany, 1990.
2. Heitler, W.; Teller, E. Time Effects in the Magnetic Cooling Method-I. *Proc. R. Soc. A Math. Phys. Eng. Sci.* **1936**, *155*, 629. [CrossRef]
3. Knight, W. Nuclear Magnetic Resonance Shift in Metals. *Phys. Rev.* **1949**, *76*, 1259. [CrossRef]
4. Korringa, J. Nuclear magnetic relaxation and resonnance line shift in metals. *Physica* **1950**, *16*, 601. [CrossRef]
5. Hebel, L.C.; Slichter, C.P. Nuclear Spin Relaxation in Normal and Superconducting Aluminum. *Phys. Rev.* **1959**, *113*, 1504. [CrossRef]
6. Dai, Y.; Kreisel, A.; Andersen, B.M. Existence of Hebel-Slichter peak in unconventional kagome superconductors. *Phys. Rev. B* **2024**, *110*, 144516. [CrossRef]
7. Bednorz, J.G.; Müller, K.A. Possible High T_c Superconductivity in the Ba-La-Cu-O System. *Z. Phys. B Condens. Matter* **1986**, *193*, 189. [CrossRef]
8. Walstedt, R.E.; Warren, J.W.W.; Bell, R.F.; Brennert, G.F.; Espinosa, G.P.; Cava, R.J.; Schneemeyer, L.F.; Waszczak, J.V. Anisotropic nuclear relaxation in $YBa_2Cu_3O_7$. *Phys. Rev. B* **1988**, *38*, 9299. [CrossRef] [PubMed]
9. Takigawa, M.; Hammel, P.C.; Heffner, R.H.; Fisk, Z. Spin susceptibility in superconducting $YBa_2Cu_3O_7$ from ^{63}Cu Knight shift. *Phys. Rev. B* **1989**, *39*, 7371. [CrossRef] [PubMed]
10. Pennington, C.H.; Durand, D.J.; Slichter, C.P.; Rice, J.P.; Bukowski, E.D.; Ginsberg, D.M. Static and dynamic Cu NMR tensors of $YBa_2Cu_3O_{7-\delta}$. *Phys. Rev. B* **1989**, *39*, 2902. [CrossRef] [PubMed]
11. Zimmermann, H.; Mali, M.; Brinkmann, D.; Karpinski, J.; Kaldis, E.; Rusiecki, S. Copper NQR and NMR in the superconductor $YBa_2Cu_4O_{8+x}$. *Phys. C Supercond.* **1989**, *159*, 681. [CrossRef]
12. Mila, F.; Rice, T.M. Analysis of magnetic resonance experiments in $YBa_2Cu_3O_7$. *Phys. C Supercond.* **1989**, *157*, 561. [CrossRef]
13. Takigawa, M.; Reyes, A.P.; Hammel, P.C.; Thompson, J.D.; Heffner, R.H.; Fisk, Z.; Ott, K.C. Cu and O NMR studies of the magnetic properties of $YBa_2Cu_3O_{6.63}$ (T_c = 62 K). *Phys. Rev. B* **1991**, *43*, 247. [CrossRef] [PubMed]
14. Bankay, M.; Mali, M.; Roos, J.; Brinkmann, D. Single-spin fluid, spin gap, and d-wave pairing in $YBa_2Cu_4O_8$: A NMR and NQR study. *Phys. Rev. B* **1994**, *50*, 6416. [CrossRef] [PubMed]
15. Haase, J.; Goh, S.K.; Meissner, T.; Alireza, P.L.; Rybicki, D. High sensitivity nuclear magnetic resonance probe for anvil cell pressure experiments. *Rev. Sci. Instrum.* **2009**, *80*, 073905. [CrossRef] [PubMed]
16. Rybicki, D.; Kohlrautz, J.; Haase, J.; Greven, M.; Zhao, X.; Chan, M.K.; Dorow, C.J.; Veit, M.J. Electronic spin susceptibilities and superconductivity in $HgBa_2CuO_{4+\delta}$ from nuclear magnetic resonance. *Phys. Rev. B* **2015**, *92*, 081115. [CrossRef]
17. Bandur, D.; Lee, A.; Nachtigal, J.; Tsankov, S.; Haase, J. Tow-Carrier Description of Cuprate Superconductors from NMR. *Condens. Matter* **2026**, *11*, 5. [CrossRef]
18. Lee, A.; Haase, J. Pseudogap and Condensation in Cuprate Superconductors from NMR. *Condens. Matter* **2026**, *11*, 19. [CrossRef]
19. Jurkutat, M.; Avramovska, M.; Williams, G.V.M.; Dernbach, D.; Pavićević, D.; Haase, J. Phenomenology of ^{63}Cu Nuclear Relaxation in Cuprate Superconductors. *J. Supercond. Nov. Magn.* **2019**, *32*, 3369–3376. [CrossRef]
20. Nachtigal, J.; Avramovska, M.; Erb, A.; Pavićević, D.; Guehne, R.; Haase, J. Temperature-Independent Cuprate Pseudogap from Planar Oxygen NMR. *Condens. Matter* **2020**, *5*, 66. [CrossRef]
21. Zheng, G.-Q.; Kitaoka, Y.; Ishida, K.; Asayama, K. Local Hole Distribution in the CuO_2 Plane of High-Tc Cu-Oxides Studied by Cu and Oxygen NQR/NMR. *J. Phys. Soc. Jpn.* **1995**, *64*, 2524. [CrossRef]
22. Jurkutat, M.; Rybicki, D.; Sushkov, O.P.; Williams, G.V.M.; Erb, A.; Haase, J. Distribution of electrons and holes in cuprate superconductors as determined from ^{17}O and ^{63}Cu nuclear magnetic resonance. *Phys. Rev. B* **2014**, *90*, 140504. [CrossRef]
23. Rybicki, D.; Jurkutat, M.; Reichardt, S.; Kapusta, C.; Haase, J. Perspective on the phase diagram of cuprate high-temperature superconductors. *Nat. Commun.* **2016**, *7*, 11413. [CrossRef] [PubMed]

24. Kowalski, N.; Dash, S.S.; Sémon, P.; Sénéchal, D.; Tremblay, A.-M. Oxygen hole content, charge-transfer gap, covalency, and cuprate superconductivity. *Proc. Natl. Acad. Sci. USA* **2021**, *118*, e2106476118. [CrossRef] [PubMed]
25. Reaney, G.L.; Kowalski, N.; Tremblay, A.-M.S.; Sordi, G. Charge gap and charge redistribution among copper and oxygen orbitals in the normal state of the emery model. *Phys. Rev. B* **2025**, *112*, 125106. [CrossRef]
26. Presland, M.; Tallon, J.; Buckley, R.; Liu, R.; Flower, N. General trends in oxygen stoichiometry effects on Tc in Bi and Tl superconductors. *Phys. C Supercond.* **1991**, *176*, 95. [CrossRef]
27. Schrieffer, J.R. *Handbook of High-Temperature Superconductivity*; Springer: Berlin/Heidelberg, Germany, 2007.
28. Jurkutat, M.; Kattinger, C.; Tsankov, S.; Reznicek, R.; Erb, A.; Haase, J. How pressure enhances the critical temperature for high temperature superconductivity in $YBa_2Cu_3O_{6+y}$. *Proc. Natl. Acad. Sci. USA* **2023**, *120*, e2215458120. [CrossRef] [PubMed]
29. Imai, T.; Slichter, C.P.; Yoshimura, K.; Katoh, M.; Kosuge, K. High-temperature 63,65Cu NQR and NMR study of the high temperature superconductor $La_{2-x}Sr_xCuO_4$ ($0 \leq x \leq 0.15$). *Phys. B Condens. Matter* **1994**, *197*, 601. [CrossRef]
30. Loram, J.W.; Mirza, K.A.; Cooper, J.R.; Tallon, J.L. Specific heat evidence on the normal state pseudogap. *J. Phys. Chem. Solids* **1998**, *59*, 2091. [CrossRef]
31. Tajima, H.; Yerin, Y.; Pieri, P.; Perali, A. Mechanisms of screening or enhancing the pseudogap throughout the two-band Bardeen-Cooper-Schrieffer to Bose-Einstein condensate crossover. *Phys. Rev. B* **2020**, *102*, 220504. [CrossRef]
32. Curro, N.J.; Imai, T.; Slichter, C.P.; Dabrowski, B. High-temperature ^{63}Cu(2) nuclear quadrupole and magnetic resonance measurements of $YBa_2Cu_4O_8$. *Phys. Rev. B* **1997**, *56*, 877. [CrossRef]
33. Sordi, G.; Sémon, P.; Haule, K.; Tremblay, A.-M.S. Strong coupling superconductivity, pseudogap, and mott transition. *Phys. Rev. Lett.* **2012**, *108*, 216401. [CrossRef] [PubMed]
34. Sordi, G.; Sémon, P.; Haule, K.; Tremblay, A.-M.S. Pseudogap temperature as a Widom line in doped Mott insulators. *Sci. Rep.* **2012**, *2*, 547. [CrossRef] [PubMed]
35. Fischer, Y.; Kugler, M.; Maggio-Aprile, I.; Berthod, C.; Renner, C. Scanning tunneling spectroscopy of high-temperature superconductors. *Rev. Mod. Phys.* **2007**, *79*, 353. [CrossRef]
36. Tallon, J.L.; Storey, J.G. Thermodynamics of the pseudogap in cuprates. *Front. Phys.* **2022**, *10*, 1030616. [CrossRef]
37. Fujita, K.; Schmidt, A.R.; Kim, E.-A.; Lawler, M.J.; Lee, D.H.; Davis, J.C.; Eisaki, H.; Uchida, S.-I. Spectroscopic Imaging Scanning Tunneling Microscopy Studies of Electronic Structure in the Superconducting and Pseudogap Phases of Cuprate High-T_c Superconductors. *J. Phys. Soc. Jpn.* **2012**, *81*, 011005. [CrossRef]
38. Damascelli, A.; Hussain, Z.; Shen, Z.-X. Angle-resolved photoemission studies of the cuprate superconductors. *Rev. Mod. Phys.* **2003**, *75*, 473–541. [CrossRef]
39. Vishik, I.M.; Lee, W.S.; He, R.-H.; Hashimoto, M.; Hussain, Z.; Devereaux, T.P.; Shen, Z.-X. ARPES studies of cuprate Fermiology: Superconductivity, pseudogap and quasiparticle dynamics. *New J. Phys.* **2010**, *12*, 105008. [CrossRef]
40. Barišić, N.; Badoux, S.; Chan, M.K.; Dorow, C.; Tabis, W.; Vignolle, B.; Yu, G.; Béard, J.; Zhao, X.; Proust, C.; et al. Universal quantum oscillations in the underdoped cuprate superconductors. *Nat. Phys.* **2013**, *9*, 761. [CrossRef]
41. Chen, X.; LeBlanc, J.P.; Gull, E. Simulation of the NMR response in the pseudogap regime of the cuprates. *Nat. Commun.* **2017**, *8*, 14986. [CrossRef] [PubMed]
42. Fujita, M.; Hiraka, H.; Matsuda, M.; Matsuura, M.; Tranquada, J.M.; Wakimoto, S.; Xu, G.; Yamada, K. Progress in Neutron Scattering Studies of Spin Excitations in High-T_c Cuprates. *J. Phys. Soc. Jpn.* **2012**, *81*, 011007. [CrossRef]
43. Birgeneau, R.J.; Stock, C.; Tranquada, J.M.; Yamada, K. Magnetic Neutron Scattering in Hole-Doped Cuprate Superconductors. *J. Phys. Soc. Jpn.* **2006**, *75*, 111003. [CrossRef]
44. Kumar, C.M.N.; Akrap, A.; Homes, C.C.; Martino, E.; Klebel-Knobloch, B.; Tabis, W.; Barišić, O.S.; Sunko, D.K.; Barišić, N. Characterization of two electronic subsystems in cuprates through optical conductivity. *Phys. Rev. B* **2023**, *107*, 144515. [CrossRef]
45. Haase, J.; Slichter, C.P.; Milling, C.T. Static Charge and Spin Inhomogeneity in $La_{2-x}Sr_xCuO_4$ by NMR. *J. Supercond.* **2002**, *15*, 339. [CrossRef]
46. Conradson, S.D.; Geballe, T.H.; Jin, C.-Q.; Cao, L.-P.; Gauzzi, A.; Karppinien, M.; Baldiozzi, G.; Li, W.-M.; Gillolo, E.; Jiang, J.M.; et al. Nonadiabatic coupling of the dynamical structure to the superconductivity in $YSr_2Cu_{2.75}Mo_{0.25}O_{7.54}$ and $Sr_2CuO_{3.3}$. *Proc. Natl. Acad. Sci. USA* **2022**, *117*, 33099. [CrossRef] [PubMed]
47. Keller, H.; Bussmann-Holder, A.; Müller, K.A. Jahn-Teller physics and high-Tc superconductivity. *Mater. Today* **2008**, *11*, 38. [CrossRef]
48. Gippius, A.A.; Antipov, E.V.; Hoffmann, W.; Lüders, K.; Buntkowsky, G. Low-frequency spin dynamics as probed by ^{63}Cu and ^{199}Hg NMR in $HgBa_2CuO_{4+\delta}$ superconductors with different oxygen content. *Phys. Rev. B* **1999**, *59*, 654.
49. Bobroff, J.; Alloul, H.; Mendels, P.; Viallet, V.; Marucco, J.F.; Colson, D. ^{17}O NMR Evidence for a Pseudogap in the Monolayer $HgBa_2CuO_{4+\delta}$. *Phys. Rev. Lett.* **1997**, *78*, 3757. [CrossRef]
50. Kambe, S.; Yasuoka, H.; Hayashi, A.; Ueda, Y. NMR study of the spin dynamics in $Tl_2Ba_2CuO_y$ (T_c = 85 K). *Phys. Rev. B* **1993**, *47*, 2825. [CrossRef] [PubMed]

51. Fujiwara, K.; Kitaoka, Y.; Ishida, K.; Asayama, K.; Shimakawa, Y.; Manako, T.; Kubo, Y. NMR and NQR studies of superconductivity in heavily doped $Tl_2Ba_2CuO_{6+y}$ with a single CuO_2 plane. *Phys. C Supercond.* **1991**, *184*, 207. [CrossRef]
52. Kambe, S.; Yoshinari, Y.; Yasuoka, H.; Hayashi, A.; Ueda, Y. ^{17}O, ^{63}Cu and ^{205}Tl NMR study of over-doped $Tl_2Ba_2CuO_y$. *Phys. C Supercond.* **1991**, *185*, 1181. [CrossRef]
53. Magishi, K.; Kitaoka, Y.; Zheng, G.Q.; Asayama, K.; Kondo, T.; Shimakawa, Y.; Manako, T.; Kubo, Y. Magnetic excitation and superconductivity in overdoped $TlSr_2CaCu_2O_{7-\delta}$: A ^{63}Cu NMR study. *Phys. Rev. B* **1996**, *54*, 10131. [CrossRef] [PubMed]
54. Auler, T.; Horvatić, M.; Gillet, J.A.; Berthier, C.; Berthier, Y.; Carretta, P.; Kitaoka, Y.; Ségransan, P.; Henry, J.Y. Normal state spin susceptibility in $YBa_2Cu_3O_{6.92}$ single crystal from ^{63}Cu and ^{89}Y nuclear magnetic resonance. *Phys. C Supercond.* **1999**, *313*, 255. [CrossRef]
55. Yoshinari, Y.; Yasuoka, H.; Ueda, Y. Nuclear Spin Relaxation at Planar Copper and Oxygen Sites in $YBa_2Cu_3O_{6.96}$. *J. Phys. Soc. Jpn.* **1992**, *61*, 770. [CrossRef]
56. Walstedt, W.R., Jr.; Bell, R.; Espinosa, G. nisotropic ^{63}Cu nuclear relaxation in magnetically oriented powdered samples of $YBa_2Cu_3O_7$. *Phys. Rev. B* **1989**, *40*, 2572.
57. Kitaoka, Y.; Ishida, K.; Fujiwara, F.; Kondo, T.; Asayama, K.; Horvatic, M.; Berthier, Y.; Butaud, P.; Segransan, P.; Berthier, C.; et al. *Strong Correlation and Superconductivity*; Müller, K.A., Cardona, M., Fulde, P., Von Klitzing, K., Queisser, H.-J., Lotsch, H.K.V., Fukuyama, H., Maekawa, S., Malozemoff, A.P., Eds.; Springer: Berlin/Heidelberg, Germany, 1989; Volume 89, pp. 262–273. [CrossRef]
58. Zimmermann, H.; Mali, M.; Bankay, M.; Brinkmann, D. Anisotropy of 63Cu Knight shift and spin-lattice relaxation in$YBa_2Cu_4O_8$. *Phys. C Supercond.* **1991**, *185–189*, 1145. [CrossRef]
59. Gerashchenko, A.P.; Piskunov, Y.V.; Mikhalev, K.; Ananyev, A.; Okuluva, K.; Verkhovskii, S.; Yakubovskii, A.; Shustov, L.; Trokiner, A. The ^{63}Cu and ^{17}O NMR studies of spin susceptibility in differently doped $Tl_2Ba_2CaCu_2O_{8-\delta}$ compounds. *Phys. C Supercond.* **1999**, *328*, 163. [CrossRef]
60. Itoh, Y.; Machi, T.; Yamamoto, A. Ultraslow fluctuations in the pseudogap states of. *Phys. Rev. B* **2017**, *95*, 094501. [CrossRef]
61. Zheng, G.-Q.; Kitaoka, Y.; Asayama, K.; Hamada, K.; Yamauchi, H.; Tanaka, S. NMR study of local hole distribution, spin fluctuation and superconductivity in $Tl_2Ba_2Ca_2Cu_3O_{10}$. *Phys. C Supercond.* **1996**, *260*, 197. [CrossRef]
62. Magishi, K.; Kitaoka, Y.; Zheng, G.-Q.; Asayama, K.; Tokiwa, K.; Iyo, A.; Ihara, H. Spin Correlation in High-T_c Cuprate $HgBa_2Ca_2Cu_3O_{8+\delta}$ with T_c = 133 K—An Origin of Tc-Enhancement Evidenced by ^{63}Cu-NMR Study. *J. Phys. Soc. Jpn.* **1995**, *64*, 4561.

Disclaimer/Publisher's Note: The statements, opinions and data contained in all publications are solely those of the individual author(s) and contributor(s) and not of MDPI and/or the editor(s). MDPI and/or the editor(s) disclaim responsibility for any injury to people or property resulting from any ideas, methods, instructions or products referred to in the content.